Texture Roughness Analysis and Synthesis via Extended Self-Similar (ESS) Model

Lance M. Kaplan, *Member, IEEE*, and C.-C. Jay Kuo, *Senior Member, IEEE*

Abstract—The 2D fractional Brownian motion (fBm) model provides a useful tool to model textured surfaces whose roughness is scale-invariant. To represent textures whose roughness is scale-dependent, we generalize the fBm model to the extended self-similar (ESS) model in this research. We present an estimation algorithm to extract the model parameters from real texture data. Furthermore, a new incremental Fourier synthesis algorithm is proposed to generate the 2D realizations of the ESS model. Finally, the estimation and rendering methods are combined to synthesize real textured surfaces.

Index Terms—Fractals, fractional Brownian motion, processes with stationary increments, terrain modeling, texture analysis, texture synthesis, random fields, roughness perception.

I. INTRODUCTION

MANY interesting textured patterns which arise in nature have certain semi-irregular structures that cannot be well modeled by traditional geometry. For instance, boxes and spheres cannot model the details of leaves and snowflakes. Recently, Mandelbrot has demonstrated how fractal geometry can be applied to mimic some natural textured patterns [26]. Mandelbrot argued that many objects in nature demonstrated similar structures at different scales and explained how self-similar patterns can be created to generate natural looking pictures. Although, many natural textures appear to be random, the randomness still exhibits a similar structure at different scales. Mandelbrot and Van Ness introduced fractional Brownian motion (fBm) as a tool to model such random phenomena [27]. The fBm process provides a nonstationary correlation which follows a stochastic self-similarity condition. Due to the similar correlation structure at all scales, fBm has significant long term correlations referred to as persistence. Since the "average" power spectrum of fBm follows a $1/f$ law [10], the fBm model provides a good basis to represent $1/f$ processes and can therefore be used to analyze data in many fields, e.g., electronics, turbulent physics, meteorology, geology and economics [6], [20], [21]. Moreover, it has been shown that the two dimensional version of fBm is a good model to generate realistic looking mountain rages, coastlines, and cloudy images [28].

A major disadvantage of fBm is that the appearance of its realizations is controlled by a single parameter H known as the Hurst parameter. The Hurst parameter controls the persistence

of fBm realizations, which is related to the visual roughness of the fBm curve [6], [22], [30]. Because of the self-similarity condition, the same parameter H determines both long- and short-term behavior of the fractal model so that the roughness of fBm realizations is invariant to scale. Even though a natural texture may exhibit similar roughness over a large range of scales, it is improper in reality to assume the roughness to be constant for arbitrary large or small scales. For instance, most of the relief of the land is formed by the movement of the earth's crust at large scales, while at the smaller scales, it seems more likely the land is smoother due to other processes such as erosion. Lewis [23] discussed many of the shortcomings of the fBm model for realism of natural scenery in the application of computer graphics. Moreover, data that appeared in [33] suggest that the landscapes are fractal for only a few scales. Another disadvantage of fBm is that the model is isotropic. For the application of generation of coastlines, the bays and peninsulas will appear roundish when using the fBm model to generate the scene. The lack of versatility for fBm to model numerous subtleties of the real world suggests that an expanded model can render many more realistic pictures.

In an effort to expand the fBm model, researchers have introduced the concept of filtered fractals as a 1D random signal model [7], [12]. Unfortunately, the filtered fractal model is difficult to generalize to 2D images. Another alternative is the long correlation model for 2D textures introduced in [18]. We consider another model for which the roughness of the realizations that can be easily parameterized. In [14], we introduced the idea of extending the definition of self-similarity to create a more general stochastic model for natural phenomena. The extended self-similarity (ESS) condition provides a scale-dependent random structure to model interesting textured signals and images.

Analogous to the relationship between the Hurst parameter and roughness, the generalized Hurst parameters provide information about multiscale roughness. Generally speaking, a slow decaying correlation function suggests a smooth function while a slow decaying power spectrum suggests a rough function due to significant high frequency components. However, these traditional analysis tools fail to provide any insight about the roughness of the curve at a particular scale. In contrast, the scale-dependent Hurst parameters in the ESS model characterize the multiscale roughness features. In this work, we are interested in texture roughness analysis and synthesis by using the ESS model. We propose an algorithm to estimate the generalized Hurst parameters of the ESS model from real image data to measure the roughness, and we study the statistics of the estimator. Then, it is shown that the generalized Hurst parameters can be manipulated to control the roughness of 2D

L.M. Kaplan is with the Radar and Communications Systems Segment, Hughes Aircraft Company, P.O. Box 92426, Los Angeles, CA 90009.
C.-C. Jay Kuo is with the Signal and Image Processing Institute and the Department of Electrical Engineering-Systems, University of Southern California, Los Angeles, CA 90089-2564; e-mail: cckuo@sipi.usc.edu.

textured surfaces at various scales, where a new incremental Fourier synthesis algorithm is used to generate the 2D realizations of the ESS model. Finally, the estimation and rendering methods are combined to synthesize real data.

The proposed new model will be useful in most applications to which fBm and fractals have been applied. These areas include terrain modeling and analysis [21], [33], classification of medical images [2], [5], [24], texture segmentation [3], [17], [19], [31], and computer graphics [26], [28]. In fact, some researchers have already considered using scale localized measurements of textures at different scales for texture classification [5], [29]. Our work provides mathematical theory as well as new estimation and synthesis algorithms for a more rigorous multiscale study of natural textures.

The paper is organized as follows. Basic results of stochastic self-similar curves and roughness are generalized to extended self-similar curves exhibiting varying roughness at different scales in Section II. A theory of 1D and 2D extended self-similar (ESS) processes is described in Section III. An estimation algorithm to measure the roughness parameters is described and tested in Section IV. In Section V, we describe an incremental synthesis method for the generation of realizations of an ESS model, and we show the visual connection between multiscale roughness and generalized Hurst parameters in Section VI. Then the estimation and synthesis algorithms are combined to render some real textures in Section VII. Finally, some concluding remarks are given in Section VIII.

II. FRACTALS AND ROUGHNESS

A. Basic Results of Fractal Curves

FBm is characterized by the self-similarity condition

$$VAR[B(t + s) - B(t)] = \sigma^2 |s|^{2H}, \quad 0 < H < 1. \quad (2.1)$$

The self-similarity condition is stationary in the sense that the power law is independent of the temporal parameter t of the random process. The value H is known as the Hurst parameter. The significance of H can be understood from both analytical and geometrical viewpoints. For instance, the Lipschitz concept describes the nature of the singularity of a function [25] where the Lipschitz exponent at a point provides information about a sudden change of the function in that position (whether the change occurred for the value of the function or it derivatives). It was shown in [9] that the Lipschitz exponent is bounded by a uniform value H for all points on a fBm curve. The smaller the value of H, the stronger the singularity and the rougher the curve. The fact $0 < H < 1$ implies that the fBm curve is too rough to be differentiable and too smooth to be discontinuous. Note that the stationarity of the self-similarity condition assures that the singularities occur almost everywhere. The Lipschitz exponent of a curve can be used to calculate the upper bound for its fractal dimension [8]. Falconer [9] showed that fBm realizations of a fractal curve with Hurst parameter H have a fractal dimension $D = 2 - H$. Since curves with a higher fractal dimension occupy more space and appear rougher, fractal geometry also supports the claim that the smaller the value H, the rougher the curve. The analytic and

geometrical interpretations of H have led researches to investigate a human's ability to classify fBm curves and surfaces based upon visual roughness. Pentland [30] and, more recently, Kumar et al. [22] have verified the relation between H and visual roughness through psychophysical studies.

B. Extended Self-Similarity

The connection between the fractal dimension and Lipschitz exponents demonstrates that the fractal dimension of a curve can be measured locally. As a result, a random fractal curve has only to follow the power scaling law of (2.1) as s approaches zero. Since the self-similarity condition is stationary (i.e., independent of t), these local measurements can be averaged at all time points to measure the local scaling exponent H (or fractal dimension $D = 2 - H$). Since the scaling law does not hold for large values of s, we consider extending the concept of self-similarity by replacing the hyperbolic function in (2.1) with a more general function $f(s)$. In other words, we define an extended self-similarity condition such that

$$VAR[B(t + s) - B(t)] = \sigma^2 f(s), \quad (2.2)$$

where $f(1) = 1$. The function $f(s)$ is known as the *structure function*. Note that the structure function is not arbitrary. Properties of the structure function can be found in [13], [32]. Since the extended self-similarity condition is still stationary, local measurements can be averaged to obtain estimates of scaling exponents. Because the local scaling exponent must be less than one (i.e., $H < 1$) to produce a curve that does not have a finite derivative in the mean square sense, it is our conjecture that processes have a fractal dimension greater than one when the term $f(s)/s^2$ diverges as s goes to zero.

In many real world applications, data is collected and presented as finite samples. For a given set of discrete data, the structure function as $s \rightarrow 0$ becomes meaningless. Algorithms which claim to measure the fractal dimension of a discrete data sequence actually measure a power law exponent over the available scales and assume that the power law is consistent for the unavailable finer scales. Instead of looking for a fractal pattern over the available scales, we propose to measure different power law exponents at different scales to provide some multiscale measure of roughness. For instance, to estimate the local Lipschitz exponent, we consider calculating a scaling law exponent over the two smallest possible scales, i.e.,

$$\tilde{H}(0) = \frac{1}{2} \log_2 \left(\frac{f(2)}{f(1)} \right).$$

If the data is subsampled by a factor of 2^m, then an appropriate value for the generalized scale dependent Hurst parameter is

$$\tilde{H}(m) = \frac{1}{2} \log_2 \left(\frac{f(2^{m+1})}{f(2^m)} \right). \quad (2.3)$$

This parameter provides clues about the apparent roughness of extended self-similar realizations at different scales. If the process happens to be fBm, then $\tilde{H}(m) = H$ for all scales. In other words, fBm has constant roughness over all scales. The following theorem puts an upper bound on $\tilde{H}(m)$.

THEOREM 1. *Let $\tilde{H}(m)$ be defined by (2.3), then*

$$\tilde{H}(m) \le 1 \quad m = 0, 1, 2, \ldots.$$

PROOF: By using the Cauchy-Schwarz inequality for the expected value operator, we can easily show that

$$f^{\frac{1}{2}}(s+t) \le f^{\frac{1}{2}}(s) + f^{\frac{1}{2}}(t).$$

By setting $s, t = 2^m$,

$$f^{\frac{1}{2}}\left(2^{m+1}\right) \le 2f^{\frac{1}{2}}\left(2^m\right).$$

Dividing both sides by $f^{\frac{1}{2}}(2^m)$ and taking the logarithm, the theorem follows. $\square$

Another similar measure of roughness over incremental lengths is also available. Since for fBm the logarithm of the structure function is $2H$ times the logarithm of the incremental length, a natural generalization of the Hurst parameter over incremental length is

$$\tilde{H}_\delta(s) = \frac{1}{2} \left. \frac{d \log(f(t))}{d \log(t)} \right|_{t=s}, \tag{2.4}$$

which is called the *differential* Hurst parameter. For sampled processes, a discrete approximation of this roughness measure yields

$$\tilde{H}_\Delta(s) = \frac{1}{2} \frac{\log(f(s+1)/f(s))}{\log((s+1)/s)}. \tag{2.5}$$

We refer to $\tilde{H}_\Delta(s)$ as the *length dependent* Hurst parameter. Note that $\tilde{H}_\Delta(s) = H$ for fBm.

III. ESS PROCESSES FOR TEXTURE MODELING

All processes with stationary increments satisfy the extended self-similar condition (2.2). In this section, we will focus on one special family known as the extended self-similar (ESS) processes and examine the 2D ESS processes for texture modeling.

Before moving to ESS processes, it is worthwhile to comment on insufficiency of signal modeling with stationary processes. A stationary process always has stationary increments. Given a 1D stationary process $B(t)$ whose correlation function $r(\tau)$ is a function only of the time lag τ, it is easy to show that the definition of the structure function (2.2) yields [32]

$$f(s) = \frac{r(0) - r(s)}{r(0) - r(1)}.$$

Most natural processes have a correlation which decays either to zero or to some constant value for large time lags, i.e., $\lim_{s \to \infty} r(s)$ exists. Therefore, the structure function $f(s)$ converges to a constant value as the incremental length s increases and, by using (2.3), one can prove that the generalized Hurst parameter $\tilde{H}(m)$ goes to zero for coarser scales, i.e., $\lim_{m \to \infty} \tilde{H}(m) = 0$. This implies that stationary processes do not have enough correlation at the coarse scales to effectively model the persistence of fBm.

A. 1D ESS Processes

To develop a model for natural textures that have decaying but significant correlation for large time lags, one must resort to a nonstationary model. We define an extended self-similar (ESS) process as a zero-mean Gaussian process that satisfies the extended self-similar condition (2.2) under the condition that at the origin,

$$B(0) = 0. \tag{3.6}$$

With the above definition, one can show that the ESS process is nonstationary since its correlation[1] is given by

$$r_B(s, t) = \frac{\sigma^2}{2}[f(s) + f(t) - f(s-t)], \quad s, t \in \mathbf{R}. \tag{3.7}$$

The restriction of the structure function is that the correlation function must be positive semidefinite. The increments of the ESS process,

$$X(k; \Delta x) = B(\Delta x(k+1)) - B(\Delta x k), \quad k \in \mathbf{Z},$$

are stationary and have the correlation function

$$r_X(k; \Delta x) = \frac{\sigma^2}{2}\left[f(\Delta x(k+1)) + f(\Delta x(k-1)) - 2f(\Delta x k)\right], \quad k \in \mathbf{Z}. \tag{3.8}$$

For most cases, as the time lag $k \to \infty$, the stationary ESS incremental correlation of (3.8) will converge to zero. Unlike the case for stationary processes, the convergent correlation function does not force the structure function to converge to a constant value. As a result, the realization of ESS processes at coarse scales can appear smooth and exhibit persistence. Note that if $f(s) = |s|^{2H}$, (3.7) defines the correlation for fBm, and (3.8) provides the stationary correlation for fBm increments. It is clear that the ESS process is a generalization of fBm.

For computer implementations, only sampled values of the ESS process can be stored and processed. We define a discrete ESS process as a zero-mean Gaussian process which satisfies (3.6) and (2.2) over the field of integer values n. Then, the finest increments of the discrete process has an incremental length $\Delta x = 1$. For 1D processes, the structure function is defined only on integer values, and the structure function is restricted to the set of function such that (3.7) is positive semidefinite over the field of integers.

Any discrete stationary processes $X(n; 1)$ can constitute increments of a discrete ESS process. The values of the discrete ESS process for positive n are found by simply summing the increments

$$B(n) = \sum_{i=0}^{n-1} X(i; 1), \quad n = 1, 2, 3, \ldots$$

As shown in [13], the structure function is related to the correlation function of the increments $X(n; 1)$ via

$$f(p) = f(p-1) + 1 + \frac{2}{r_X(0; 1)}\sum_{k=1}^{p-1} r_X(k; 1), \quad p = 2, 3, \ldots \tag{3.9}$$

or

---

1. In this paper, the correlation function for the random process $B(t)$ is $r_B(s, t) = E[B(s)B(t)]$, and if $B(t)$ is stationary, then $r_B(\tau) = r_B(t + \tau, t)$.

$$f(p) = p + \frac{2}{r_X(0;1)} \sum_{k=1}^{p-1} (p-k) r_X(k;1), \quad p = 2, 3, \ldots \quad (3.10)$$

where $f(0) = 0$, $f(1) = 1$, and $f(-p) = f(p)$.

Note that the correlation function for fBm increments is controlled by the values of the Hurst parameter. For instance, the increments are positively correlated when $H > 1/2$, negatively correlated when $H < 1/2$, and uncorrelated $H = 1/2$. Similar bounds can be placed on the generalized Hurst parameters for many ESS processes as stated by the following theorem.

THEOREM 2. *Let $\tilde{H}$ and $\tilde{H}_\Delta$ be defined in (2.3) and (2.5), respectively, and let $X_f(k; 1)$ be the finest scale increments of a discrete ESS process that has a correlation $r_{X_f}(k; 1)$ defined by (3.8).*

(a) *If $r_X(k; 1) \geq 0$ for all k and $r_X(k)$ is monotonically decreasing, then for all scales $m = 0, 1, 2, \ldots$ and incremental lengths $s = 1, 2, \ldots,$*

$$1/2 \leq \tilde{H}(m), \ \tilde{H}_\Delta(s) \leq 1,$$

(b) *and if $r_X(k; 1) \leq 0$ for $|k| > 0$ and $\left| r_{X_f}(k) \right|$ is monotonically decreasing, then*

$$0 \leq \tilde{H}(m), \ \tilde{H}_\Delta(s) \leq 1/2.$$

The proof of Theorem 2 is given in the appendix.

B. 2D ESS Processes

To model 2D textured surfaces, we define a 2D ESS process $B(\vec{k})$ to be a zero-mean multivariate Gaussian process such that at the origin $B(\vec{0}) = 0$ and the variance of the increments of $B(\vec{k})$ follows a power law of

$$\text{VAR}\left[B(\vec{k}+\vec{l}) - B(\vec{k}) \right] = \sigma^2 f\left(\|\vec{l}\|_R \right), \quad (3.11)$$

where $\vec{l}$ and $\vec{k}$ denote arbitrary displacement vectors with

$$\|\vec{k}\|_R = \sqrt{\vec{k}^T R \vec{k}},$$

and R is a positive definite matrix. If $f(l) = |l|^{2H}$ for $0 < H < 1$ and $R = I$, then $B(\vec{k})$ is simply the 2D fBm. In general, if $R = I$, then the 2D ESS process is isotropic. Similar to the 1D case, the 2D ESS process is not stationary, and its correlation function is

$$r_B(\vec{t}, \vec{s}) = \frac{\sigma^2}{2} \left[f\left(\|\vec{t}\|_R \right) + f\left(\|\vec{s}\|_R \right) - f\left(\|\vec{t} - \vec{s}\|_R \right) \right]. \quad (3.12)$$

A discrete 2D ESS process is defined such that $\vec{t}, \vec{s} \in Z^2$. Unlike the 1D case, the structure function must be defined over noninteger values. The constraint for the structure function is that (3.12) is positive semidefinite over the 2D integer lattice.

Each normalized 1D slice of a 2D ESS process forms a 1D ESS process. Specifically, given a normalized directional vector $\vec{n}$ such that $\|\vec{n}\|_I = 1$ and an offset $\vec{o}$, the normalized process $B_{\vec{n}, \vec{o}}(k) = B(k\vec{n} + \vec{o}) - B(\vec{o})$ has a structure function

$$f_{\vec{n}}(s) = \frac{f\left(s \|\vec{n}\|_R \right)}{f\left(\|\vec{n}\|_R \right)}.$$

Obviously, the increments of the 1D ESS slice, i.e., $X(k) = B((k+1)\vec{n} + \vec{o}) - B(k\vec{n} + \vec{o})$, are stationary, and these increments are referred to as first order increments of the 2D ESS process. Moreover, the second order increments of a 2D ESS process are defined as

$$X(\vec{k}) = B(\vec{k}) + B(\vec{k} + (1, 1)^T) - B(\vec{k} + (1, 0)^T) - B(\vec{k} + (0, 1)^T). \quad (3.13)$$

It can be shown that the second order increments also form a stationary process.

C. Parameterized ESS Models

The structure function determines the appearance of the 2D random model as discussed in Section II. For example, the hyperbolic structure function $f(s) = |s|^{2H}$ defines a subset of ESS processes known as the fBm. The Hurst parameter characterizes the fBm, and the roughness of the fBm process is invariant to scale. In this section, we consider alternative parameterizations of the structure function. We do restrict our models to discrete ESS processes, because they are intended to be used to create or analyze computer data. Two examples of structure functions are given below.

EXAMPLE 1. Asymptotic FBm. A structure function that provides a model whose long term behavior is like the fBm while short term correlations are altered is

$$f(l) = (1 - A)\frac{\rho^{|l|} - 1}{\rho - 1} + A|l|^{2H}, \quad (3.14)$$

where $0 \leq \rho < 1$, $0 \leq H \leq 1$, and A is bounded by values that depends on ρ and H. The parameter A is the smoothness parameter that determines how correlated the process is in the short term, H is the asymptotic Hurst parameter or persistence parameter which measure how smooth coarse representations of the random field appears, and ρ is the smoothness capacitance because it measure how quickly the fine scale smoothness is lost. In fact, the values of $\tilde{H}(m)$ for such a structure function converge to H as $m \to \infty$. The rate of convergence is dependent of the value of ρ. We refer to the resulting ESS process as *asymptotic* fBm (afBm).

EXAMPLE 2. Delta Hurst. The delta Hurst model is parameterized by the length dependent Hurst parameters $\tilde{H}_\Delta(s)$ for $s = 1, \ldots, S$. The structure function is defined as

$$f(s) = \begin{cases} 0 & \text{if } s = 0 \\ \prod_{i=1}^{\lfloor |s| \rfloor - 1} \left(\frac{i+1}{i} \right)^{2\tilde{H}_\Delta(i)} \left(\frac{|s|}{\lfloor |s| \rfloor} \right)^{2\tilde{H}_\Delta(\lfloor |s| \rfloor)} & \text{if } 1 \leq |s| < S \\ \prod_{i=1}^{S-1} \left(\frac{i+1}{i} \right)^{2\tilde{H}_\Delta(i)} \left(\frac{|s|}{S} \right)^{2\tilde{H}_\Delta(S)} & \text{if } S \leq |s| \end{cases} \quad (3.15)$$

where $\lfloor \cdot \rfloor$ represents the greatest lower integer. The length de-

pendent Hurst parameters are completely determined by the model parameters for lengths $s = 1, \ldots, S$. When $s > S$, $\tilde{H}_A(s) = \tilde{H}_A(S)$. The modeler has more control of the roughness for this model than the afBm model. One potential drawback to the model is that the differential Hurst parameter $\tilde{H}_\delta(s)$ defined by (2.4) is constant and equal to $\tilde{H}_A(\lfloor s \rfloor)$ for $\lfloor s \rfloor < s < \lfloor s \rfloor + 1$. Then, the values of $\tilde{H}_\delta(s)$ may jump for integer values of s. As demonstrated in [13], the length dependent Hurst parameters should not change drastically over s.

IV. ESTIMATION OF THE GENERALIZED HURST PARAMETERS

For texture analysis and synthesis applications, the estimation of the generalized Hurst parameters provides important information. In this section, we present a straightforward algorithm to measure the scale dependent Hurst parameter and demonstrate the quality of the estimator through numerical simulations. The algorithm presented in this section assumes that the image is isotropic. However, it can be easily generalized to the nonisotropic case.

To estimate the generalized Hurst parameters of an isotropic image, the average energy of the nonoverlapping horizontal and vertical increments for available scales are calculated. Then, the scale dependent Hurst parameters are estimated by using the logarithm of the ratio of the energy at different scales. The algorithm is detailed below.

ALGORITHM 1. ESTIMATION OF GENERALIZED HURST PARAMETERS FROM IMAGES.

Let $B(x, y)$ be an isotropic ESS texture of size $N \times N$, then to calculate $\tilde{H}(m)$,

1) *Calculate the incremental energy for scales* $m = 0, 1, \ldots,$ $\log_2(N) - 1$:

$$\hat{E}_x(m) = \frac{2^m}{N^2} \sum_{x=0}^{N/2^m - 1} \sum_{y=0}^{N-1} \left| B(2^m(x+1), y) - B(2^m x, y) \right|^2,$$

$$\hat{E}_y(m) = \frac{2^m}{N^2} \sum_{x=0}^{N-1} \sum_{y=0}^{N/2^m - 1} \left| B(x, 2^m(y+1)) - B(x, 2^m y) \right|^2.$$

2) *Estimate the generalized Hurst parameters for scales* $m = 0, 1, \ldots, \log_2(N) - 2$:

$$\hat{\tilde{H}}(m) = \frac{1}{2} \log_2 \left(\frac{\hat{E}_x(m+1) + \hat{E}_y(m+1)}{\hat{E}_x(m) + \hat{E}_y(m)} \right).$$

Note that nonisotropic measurements can be made by considering separate ratios of $\hat{E}_x(m)$ and $\hat{E}_y(m)$ to estimate x and y directed values for $\tilde{H}(m)$. In addition, other incremental energy calculations for other lag directions may be necessary depending on the orientation of the nonisotropic texture.

To test the robustness of the estimation algorithm we calculated the mean and standard deviation of the generalized Hurst parameter estimates over 64 independent realization of 128×128 2D ESS images. The images were rendered by the

incremental synthesis method detailed in Section V. The test was performed for eight different afBm models which were chosen to represent numerous situations of persistence (i.e., $\tilde{H}(m) > 1/2$), antipersistence (i.e., $\tilde{H}(m) < 1/2$), and nonpersistence (i.e., $\tilde{H}(m) = 1/2$) at both the fine and coarse scales. Table I shows the parameters for the eight afBm models. Note that the first three test cases represent the fBm subset of afBm. The actual and estimated mean of the scale dependent Hurst parameters are displayed in Fig. 1. The error bars in the figure represent the standard deviation of the Hurst estimate. Obviously, the standard deviation of $\hat{\tilde{H}}(m)$ increases as the scale becomes coarser because less measurements are available. The figure shows that the estimation algorithm provides close to unbiased results, and the standard deviation is low enough for most scales to provide a good classification feature. It is clear that for the coarsest scale, the estimator underestimates the generalized Hurst parameter, and the bias is larger for more persistent models.

TABLE I
PARAMETER VALUES FOR THE EIGHT afBm TEST CASES

Test	H	ρ	A
1	0.7500	0.0000	1.0000
2	0.5000	0.0000	1.0000
3	0.2500	0.0000	1.0000
4	0.6000	0.2182	1.6802
5	0.5000	0.3704	2.6383
6	0.3000	0.2649	7.0421
7	0.1000	0.0061	11.4524
8	0.3500	0.8069	0.2261

TABLE II
THE HURST PARAMETER ESTIMATE USING THE fBm MODEL
FOR THE EIGHT TEST CASES

Test Case	True H	$\hat{H}$ Mean	$\hat{H}$ Std
1	0.75	0.7241	0.0422
2	0.50	0.4938	0.0227
3	0.25	0.2474	0.0168
4	—	0.6812	0.0316
5	—	0.6667	0.0229
6	—	0.6212	0.0217
7	—	0.4191	0.0138
8	—	0.3150	0.0147

The above estimation algorithm can be modified to calculate the Hurst parameter for true fBm data more accurately. To perform the modification, the average energy of the horizontal and vertical increments at the same scales can be averaged to provide an estimate of the structure function. The structure function for fBm is related to scale m by

$$E(m) = \sigma^2 2^{2Hm}.$$

Then H can be estimated via the slope of the $\log_2(E(m))$ versus $\log_2(m)$, where the slope is calculated by performing linear regression using weighted least squares to take into account that more measurements are available for the finer scales. The modification was tested on the first three test cases which represent 2D fBm images. Table II shows the mean and standard
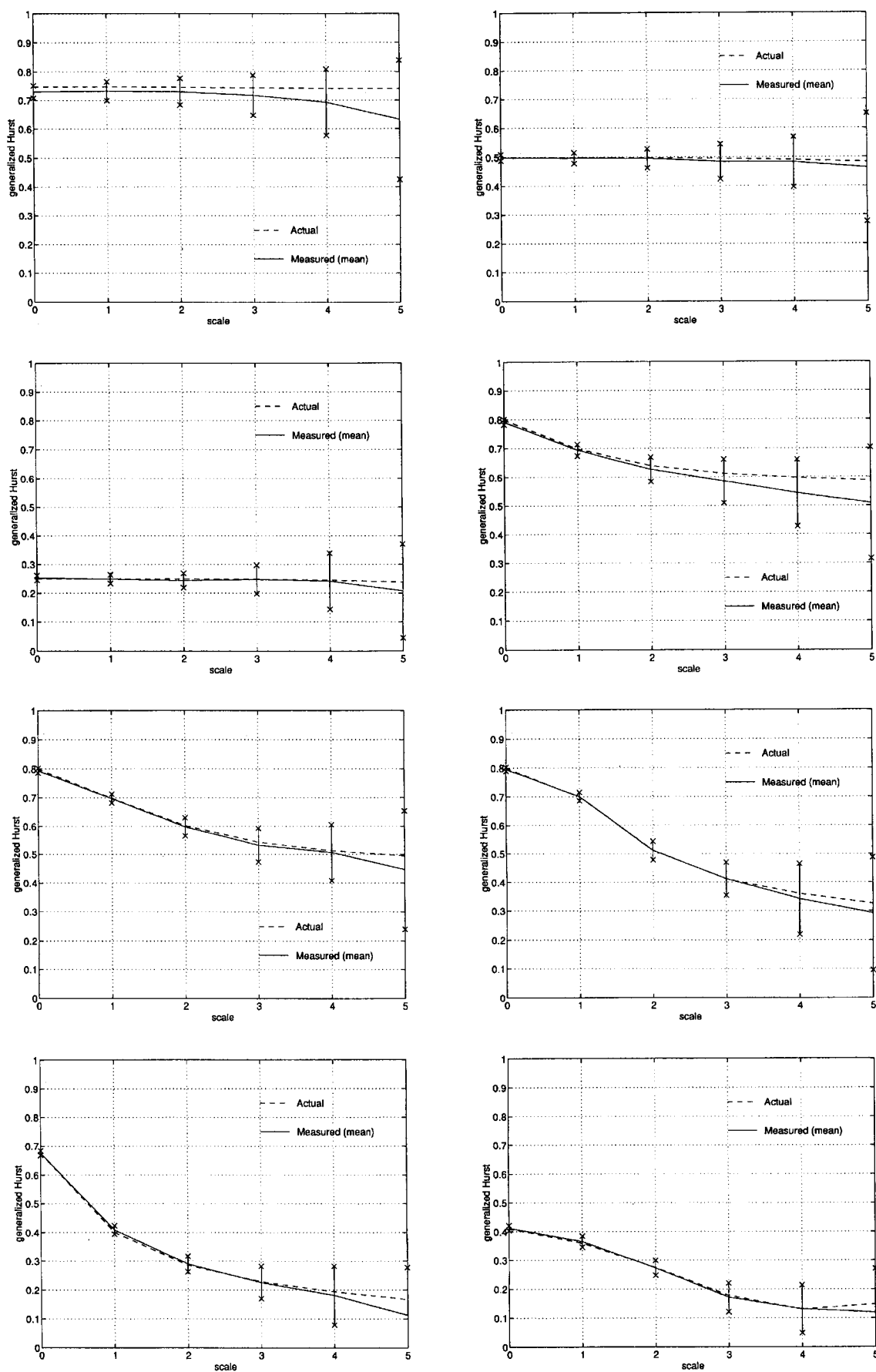
Fig. 1. Accuracy of the scale dependent Hurst parameter estimation algorithm. Left column, top to bottom: Test 1, Test 3, Test 5, Test 7; Right column, top to bottom: Test 2, Test 4, Test 6, Test 8.

deviation of the Hurst parameter for the three fBm test cases and the other five test cases. Even though the method underestimates the Hurst parameter for persistent fBm, the overall performance is very good. For nonfBm data, the results are not informative except that they should fall between the values of $\tilde{H}(m)$ corresponding to the finest and coarsest scales.

V. SYNTHESIS OF ESS PROCESSES

The 1D and 2D ESS processes can be synthesized through the use of Cholesky decomposition. The Cholesky decomposition has been used to create 1D fBm in [24] and to create 2D fBm in [11]. The difficulty of using the Cholesky algorithm includes numerical complexity and memory requirements. For example, to create a 1D ESS process of length N, the computational complexity of the Cholesky method is $O(N^3)$ and the memory requirements are $O(N^2)$. This becomes even worse for 2D ESS synthesis, i.e., to create an $N \times N$ 2D ESS process requires $O(N^6)$ computations and $O(N^4)$ storage units. Another problem is that if the correlation is not positive definite, the Cholesky decomposition will break down and provide no output.

To generate ESS realizations, we will use a method called the incremental Fourier synthesis. The advantages of this new method over traditional Fourier synthesis is documented in [15]. For the generation of 1D ESS processes, the algorithm requires $O(N\log_2(N))$ operations with memory requirements of $O(N)$ because the method take advantage of the fast Fourier transform (FFT). Similarly, for a 2D ESS process, the computation complexity is $O(N^2\log_2(N))$ and the memory requirements are $O(N^2)$. While the method does not generate a process based on the exact statistics of the ESS process, the method does creates realization with statistics that are very close to the intended ESS process. Moreover, if the correlation of the ESS process is not positive semidefinite, the algorithm still attempts to create a positive definite process whose statistics are as close as possible to the intended ESS process. In fact, a major discrepancy between the synthesized and intended statistics is an indication that the intended ESS process is not well defined.

The basic idea behind incremental Fourier synthesis is to create the stationary increments through Fourier synthesis. Traditional Fourier synthesis attempt to create the nonstationary process directly. The new method exploits the fact that the discrete Fourier transform (DFT) represent the Karhunen Loève transformation for a discrete periodic stationary random processes. The method, however, cannot create exact realizations because the target correlation functions of the increments are considered to have compact support and are periodically extended to form the periodic process. As a result, the values of the target power spectra may have some small negative values which are forced to be zero in the actual power spectrum. The 1D incremental Fourier synthesis algorithm is stated below.

ALGORITHM 2. 1D INCREMENTAL FOURIER SYNTHESIS.

1) *Create white noise processes such that for*

$$k = 0, \ldots, N, \; \hat{W}(k) \sim N(0, 1), \; \phi(k) \sim Uniform[0, 2\pi),$$

and $\phi(0) = \phi(N) = 0$.

2) *Calculate the target correlation function $R(n)$ for $k = 0$, ..., N by (3.8) for $\Delta x = 1$, and for $k = N + 1$, ..., $2N - 1$ let $R(n) = R(2N - n)$.*

3) *Calculate the target power spectrum $\hat{R}(k)$ by taking the FFT of $R(n)$.*

4) *Define the actual positive semidefinite power spectrum of the synthesized increments by*

$$\hat{S}(k) = \begin{cases} 0 & \text{if } \hat{R}(k) < 0 \\ \hat{R}(k) & \text{otherwise} \end{cases}.$$

5) *Synthesize the FFT coefficients of the increments by*

$$\hat{X}(k) = \begin{cases} \sqrt{N\hat{S}(k)}\hat{W}(k)e^{j\phi(k)} & \text{for } k = 0, \ldots, N \\ \hat{X}^*(2N - k) & \text{for } k = N+1, \ldots, 2N-1 \end{cases}.$$

6) *Calculate the increments by taking the inverse FFT of $\hat{X}(k)$.*

7) *Calculate the ESS process by summing up the increments for $n = 1, \ldots, N - 1$,*

$$B(0) = 0,$$

$$B(n) = B(n - 1) + X(n - 1).$$

The advantage of the incremental Fourier method is that the actual correlation function of the synthesized increments is found by simply taking the inverse FFT of the actual power spectrum $\hat{S}(k)$. Then, by using (2.3) and (3.10), the actual values of the generalized Hurst parameters for the synthesized fields are available.

The 2D incremental Fourier synthesis algorithm creates both the stationary first and second order increments of a 2D ESS process by Fourier synthesis. The first order increments are summed to generate the values of the 2D ESS process along the x and y axis, and the second order increments are summed to fill the remaining 2D lattice. The first and second order increments can not be generated independently. The details of the 2D algorithm are given in [15] for the case of fBm and in [16] for the general ESS model. For the sake of brevity, the 2D algorithm will not be repeated here.

VI. TEXTURE ROUGHNESS ANALYSIS WITH ESS MODEL

By using the generation procedure described in the previous section, the relationship between the generalized Hurst parameter and textured surface roughness can be verified. Recall that the smoothness (or roughness) of the textured surface is directly linked to a larger (or smaller) value of the generalized Hurst parameter. To demonstrate this concept, we generated two 2D processes of size 512×512 with the same random seed. They are:

1) fBm with $H = 0.4$ (i.e., afBm with $H = 0.4$, $\rho = 0$, and $A = 1$) and

2) afBm with $H = 0.4$, $\rho = 0.4339$, and $A = 6.6684$.

Figs. 2a and b show the scale dependent Hurst parameters for these two cases at various scales. The generalized Hurst parameters are similar for the two processes at coarser scales (larger m), but different at finer scales (smaller m). Figs. 3 and 4
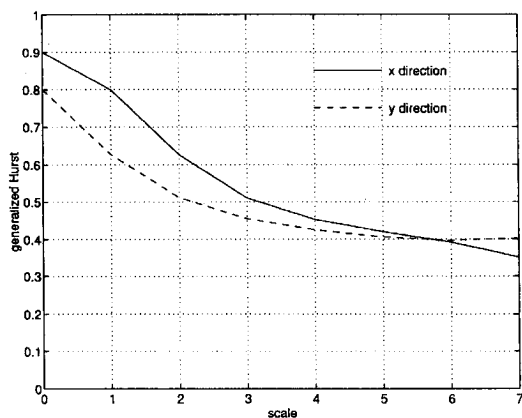
show the textured images of the four processes at two scales. At each scale, the resolution of the picture is 64 × 64, and each picture is scaled so that the dynamic range of the pixel values cover all 64 gray level values. As expected, at the coarse scales the two processes appear identical, and at the finer scales the afBm process is smoother.
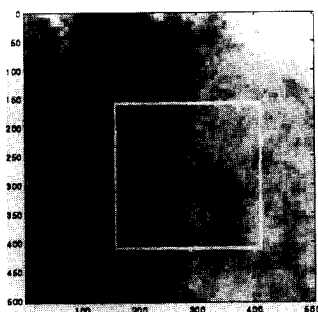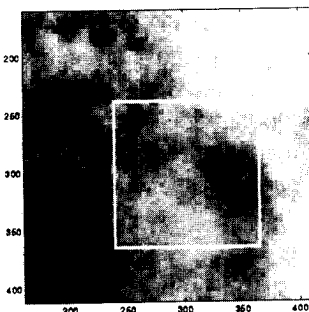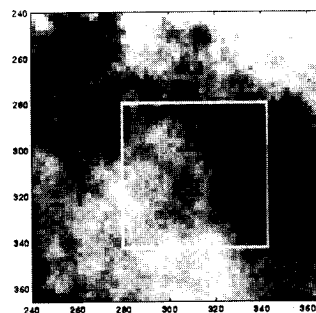

(a)

(b)
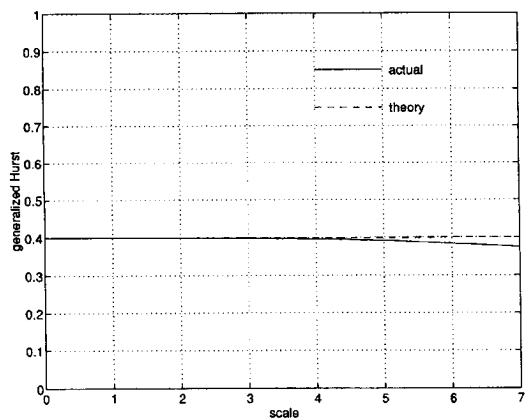
(a)
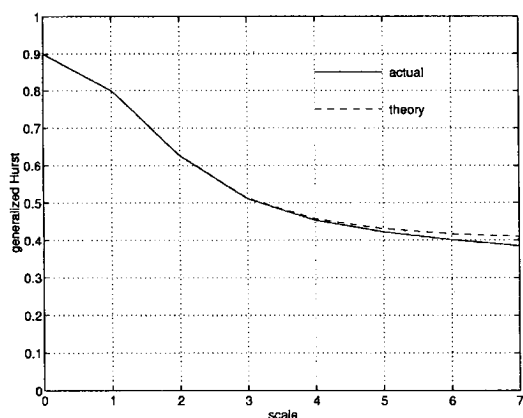
(b)

(c)

Fig. 2. Scale dependent Hurst parameters for 2D random processes: (a) 2D fBm ($H = 0.4$), (b) isotropic 2D afBm ($H = 0.4$, $\rho = 0.4339$, and $A = 6.6684$), and (c) nonisotropic 2D afBm ($H = 0.4$, $\rho = 0.4339$, and $A = 6.6684$).

(c)
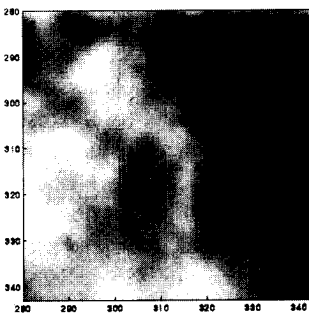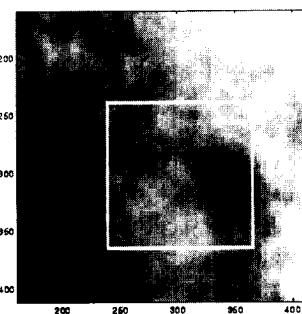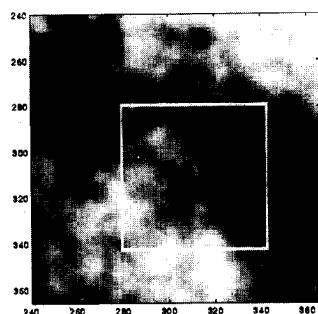

(d)

Fig. 3. Zooming into an fBm texture with $H = 0.4$: a sampled every eight units ($m = 3$), (b) sampled every four units ($m = 2$), (c) sampled every two units ($m = 1$), and (d) sampled every unit ($m = 0$).
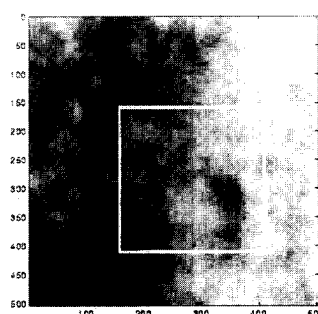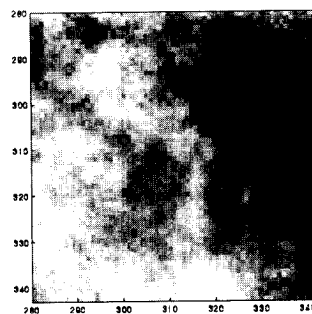

(a)

(b)

(c)

(d)

Fig. 4. Zooming into an afBm texture with $H = 0.4$, $\rho = 0.4339$, and $A = 6.6684$: (a) sampled every eight units ($m = 3$), (b) sampled every four units ($m = 2$), (c) sampled every two units ($m = 1$), and (d) sampled every unit ($m = 0$).

(a)   (b)

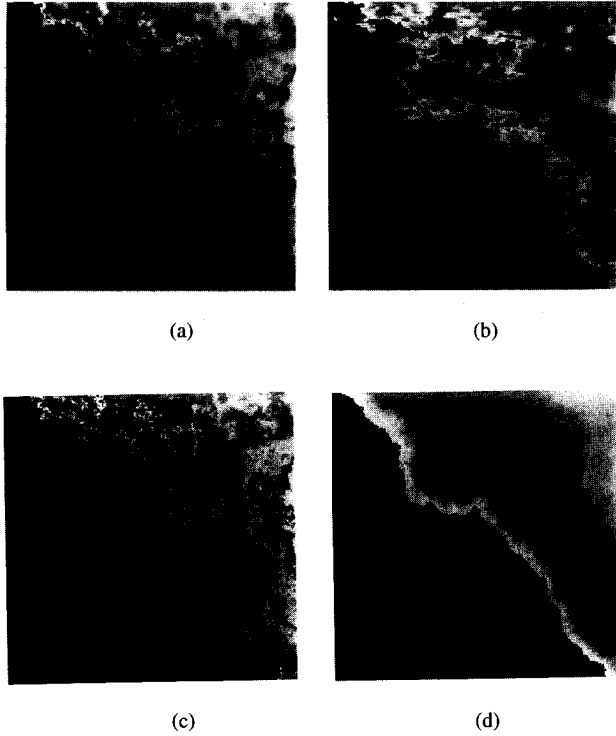(c)   (d)

Fig. 5. Comparison of different coastline models generated by the same seed: (a) an isotropic afBm model, (b) a nonisotropic afBm model, (c) a rough fBm model, and (d) a smooth fBm model.

To further examine the versatility of the ESS model, we represent the surface of a 2D ESS process as coastlines so that all values which fall below a given sea level are represented as black. The land is represented as lighter shades of gray that depend on the elevation of the surface. As before, we used the 2D afBm model with $H = 0.4$, $\rho = 0.4339$, and $A = 6.6684$, of size 256×256 to synthesis an isotropic and a nonisotropic processes. For the nonisotropic process, we choose

$$\mathbf{R} = \begin{pmatrix} 1 & 0 \\ 0 & 4 \end{pmatrix}.$$

The scale dependent Hurst values for the isotropic and nonisotropic processes are given if Figs. 2b and c. Figs. 5a and b represent the coastlines of isotropic and nonisotropic afBm, respectively. The two figures show that the coastlines of the resulting processes appear smooth and natural at the finer scales. The smaller values for the scale dependent Hurst values at the coarser scales yield the interesting bay formations. The smaller values for the scale dependent Hurst parameters in the y direction of the nonisotropic afBm model indicate that the surface is rougher in the y direction so that the bays and peninsulas will be longer in the x direction. These two facts are verified in Fig. 5. Figs. 5c and d show fBm with $H = 0.4$ and $H = 0.75$, respectively. The images in Fig. 5 were generated by the same seed, and the figure demonstrates that at coarse scales, the isotropic afBm process with $H = 0.4$ has almost the same coastline as fBm with $H = 0.4$. At the finer scales, however, the afBm process is smoother and looks more realistic. Fig. 5b shows that changing the value of $\mathbf{R}$ allows for less roundish bays and peninsulas, and Fig. 5d shows that fBm with

larger values of H are smooth enough at the fine scales to appear real. However, these fBm processes are too smooth at the coarser scales to provide interesting bay formations.

Finally, we compare the effect of zooming into the coastlines of fBm and afBm that appear similar at the coarse scales in Figs. 6 and 7. The images in Figs. 6 and 7 were generated using the same random seed. The self-similarity of fBm is evident in Fig. 6 where the overall roughness of the coastline is independent of the scale. Fig. 7 verifies that at the finer scales the afBm can be designed to be much smoother than at coarser scales.
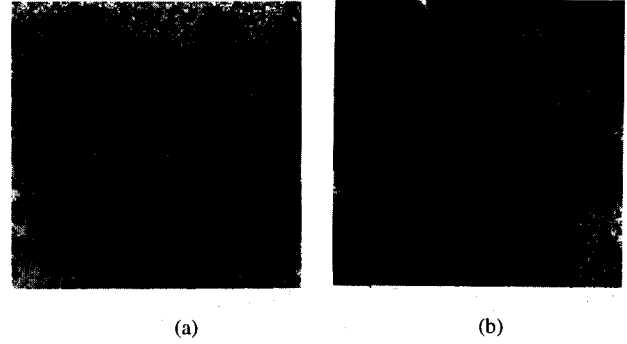

(a)   (b)

Fig. 6. FBm with $H = 0.4$: (a) the coastline and (b) zoom in of the coastline.
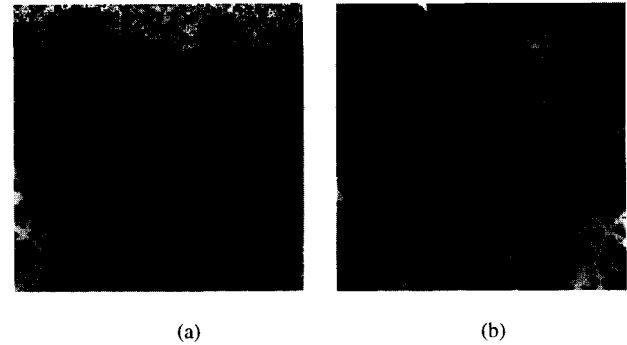

(a)   (b)

Fig. 7. AdBm with $H = 0.4$, $\rho = 0.5436$, and $A = 9.8139$: (a) the coastline and (b) zoom in of the coastline.

VII. REAL TEXTURE RENDERING

The problem of real texture rendering involves measuring features or parameters from real textured data and using these parameters to synthesize textures so that the synthesized texture appear similar to the real texture. We investigate the isotropic afBm and delta hurst models to render real isotropic textures based upon the scale dependent Hurst parameters in this section. The current work considers the synthesis of textures that exhibit the decaying but significant correlation which result in "cloudy" textures. Examples of "cloudy" textures include mammographic images, terrain models (when the elevation is viewed as a gray level), and pictures of fire, dust, clouds, and smoke. The current work does not consider the synthesis of processes that contain any dominate harmonics which result in a deterministic structure that propagates through the structure. Examples of the more structured textures include many of the textures found in the Brodatz album including wood, cloth, sand, and netting [1]. Chellappa and

Kashyap have demonstrated how to use the noncausal autoregressive (NCAR) models to render such textures [4]. The NCAR model is stationary and thus unable to capture the decaying but significant correlations (or $1/f$ effect) of persistent textures (see Section III). Therefore, the NCAR and ESS models coexist to represent two different classes of natural textures.

To render an ESS model that did capture some periodic effects of a texture would require measurements of the length dependent Hurst parameters or structure function. At least for 1D signals, the complete discrete structure function can be rebuilt from these parameter values, and a discrete structure function can represent periodic signal [13]. The problem with using the $\tilde{H}_\Delta(s)$ measurements is that half of the parameter values require estimation of the structure function at a scale which exceeds the maximum scale estimated by Algorithm 1. Based on the results of Section IV, the variance of the $\tilde{H}_\Delta(s)$ estimates for these lengths will be too high for the estimates to be reliable. Therefore, the paper only considers measurements of $\tilde{H}(m)$.

A. Calculation of Model Parameters

In Section IV, we described a method to calculate the scale dependent Hurst parameters which can be further used to calculate the parameters of the afBm and delta Hurst models. To calculate the parameters of the afBm model, one assumes that the coarsest scale value of $\tilde{H}(m)$ represents the asymptotic Hurst parameter for the afBm model (i.e., H). Then, for many cases, one can choose values for the parameters of afBm so that the fine scale roughness values of $\tilde{H}(0)$ and $\tilde{H}(1)$ are predetermined for a given value of H. It turns out that the value of ρ can be calculated by solving for the roots of the following third order polynomial

$$a\rho^3 + a\rho^2 + (a+b)\rho + (a+b+c) = 0,$$

where

$$a = 2^{2\tilde{H}(0)} - 2^{2H},$$

$$b = 2^{4H} - 2^{2(\tilde{H}(0)+\tilde{H}(1))},$$

$$c = 2^{2(H+\tilde{H}(0)+\tilde{H}(1))} - 2^{2(2H+\tilde{H}(0))}.$$

Then, A is determined by

$$A = \frac{2^{2\tilde{H}(0)} - (1+\rho)}{2^{2H} - (1+\rho)}.$$

Note that the combinations of $\tilde{H}(0)$, $\tilde{H}(1)$, and H can be represented by the afBm model only if one root of the third order polynomial is between zero and one. For example, if one wants $H = 0.4$, $\tilde{H}(0) = 0.9$, and $\tilde{H}(1) = 0.8$, then one would set $\rho = 0.4339$ and $A = 6.6684$ (see Fig. 2).

A drawback of the afBm model is that the method presented above will only use the three parameters of afBm to fit the actual to the measured $\tilde{H}(m)$ for exactly two points. Moreover, there is no guarantee that a model exists to fit the measured data. In contrast, the delta hurst parameter has an arbitrary number of parameters to fit the generalized Hurst plot

exactly.

To fit the delta Hurst model to the measured data, one must find values of $\tilde{H}_\Delta(s)$ for $s = 1, \ldots, S$ where $S = 2^{M+1}$ and M is the coarsest measured scale. By substituting the delta Hurst structure function of (3.15) into (2.3), one can compute the relation between the scale and length dependent Hurst parameter to be

$$\hat{\tilde{H}}(m) = (m+1)\tilde{H}_\Delta\left(2^{m+1} - 1\right) - m\tilde{H}_\Delta\left(2^m\right)$$

$$+ \sum_{i=2^m+1}^{2^{m+1}-1} \log_2(i)\left[\tilde{H}_\Delta(i-1) - \tilde{H}_\Delta(i)\right], \quad (7.16)$$

for $m = 0, \ldots, M$. As shown in [13], the length dependent Hurst parameters should not change abruptly for the delta Hurst model to be well defined. We choose to make $\tilde{H}_\Delta(s)$ vary linearly with respect to the logarithm of s for constant scales, i.e.,

$$\tilde{H}_\Delta(s) = a_m \log_2(s+1) + b_m \quad \text{for } s = 2^m - 1, \ldots, 2^{m+1} - 1. \quad (7.17)$$

By substituting (7.17) into (7.16), one can show after some algebra that

$$a_m = \frac{\hat{\tilde{H}}(m) - \tilde{H}_\Delta\left(2^m\right)}{m^2 + m + 1 - m\log_2\left(2^m + 1\right) + \sum_{i=2^m+1}^{2^{m+1}-1} \log_2(i)\left[\log_2(i) - \log_2(i+1)\right]},$$

$$b_m = \tilde{H}_\Delta\left(2^m - 1\right) - ma_m,$$

for $m = 1, \ldots, M$. By initializing $\tilde{H}_\Delta(1) = \hat{\tilde{H}}(0)$, the values of $\tilde{H}_\Delta(s)$ for $s = 2, \ldots, 2^{M+1} - 1$ can be calculated.

B. Experiments

Both the afBm and delta Hurst models can be used to render textures. We will only present the results of the delta Hurst model in this section. To render a texture of size $N \times N$, the coarsest scale available for $\tilde{H}(m)$ is $M = \log_2(N) - 1$. The first M values of $\tilde{H}(m)$ are estimated by Algorithm 1, and $\tilde{H}(M)$ is set equal to $\tilde{H}(M-1)$. Then, the parameters for the delta Hurst model are calculated, and the 2D ESS model is rendered based upon the delta Hurst structure function. Since the ESS model represents an improved model over traditional fBm for the representation of persistent textures, we compare the rendered ESS result to a rendered fBm textures. Specifically, we generate a 2D fBm texture based upon the measured fBm Hurst value for the real data.

For an illustration of terrain modeling, we used data from a digital elevation model (DEM) provided by the U.S. Geological Survey. A DEM provides elevation levels for a square lattice of land. To visualize the DEM, we will represent the DEM as a coastline image to distinguish the contours of the land. The DEM used represents Allens Park in Rocky Mountain National Park in Colorado. The generalized Hurst plots for the real and rendered DEM appear in Fig. 8. The real, ESS, and fBm coastlines are shown in Fig. 9. Both the actual DEM and rendered ESS model display large bays, and the fine scale coastline for both textures appear very smooth. The rendered

fBm coastline, on the other hand, does not exhibit the large bays because H is too large to model the coarse scale roughness of the DEM. At the same time, the fine scale coastline of the fBm model appears rougher than the DEM and ESS model. Obviously, the ESS model is better than the fBm model for capturing features of the DEM at all available scales. In other words, the ESS model provides an improved model to synthesize and analyze terrains.
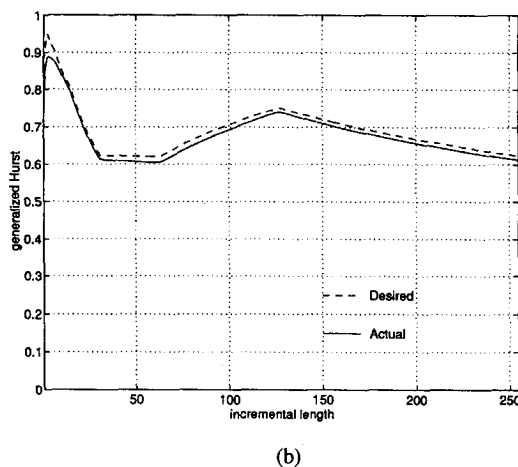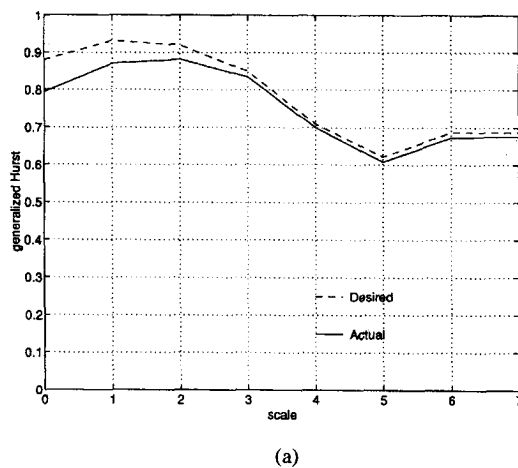

(a)

Fig. 8. Generalized Hurst parameters for the Allens Park, CO DEM: (a) $\tilde{H}(m)$ and (b) $\tilde{H}_\Delta(s)$.

Next, we investigate how the ESS model is better than fBm at capturing some of the effects of one of the random Brodatz texture. We rendered the pressed cork texture (D4) because this texture represents a random isotropic texture which does not exhibit any dominant harmonics. The generalized Hurst plots for the real and rendered textures are shown in Fig. 10, and since the generalized Hurst parameters converge to zero, the plot suggests that pressed cork might be a stationary texture. The real, ESS, and fBm textures are provided in Fig. 11. The ESS model was able to represent some of the granularity of the original texture, but the model can not represent the deterministic texel primitive of the cork. The fBm image fails to resemble the cork texture. The fBm image appears too cloudy, and the image does not exhibit the larger grainy structure of the ESS and cork textures.
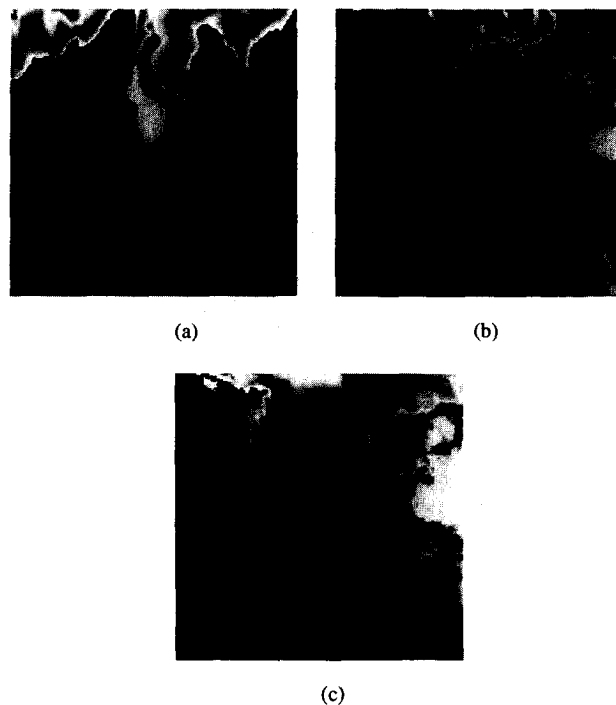

(a)   (b)

(c)

Fig. 9. Comparison of real and synthesized DEM data: (a) Allens Park, CO DEM, (b) synthesized ESS model, and (c) synthesized fBm model ($H = 0.85$).
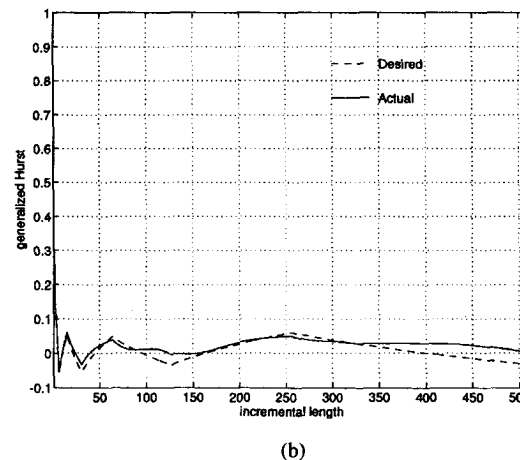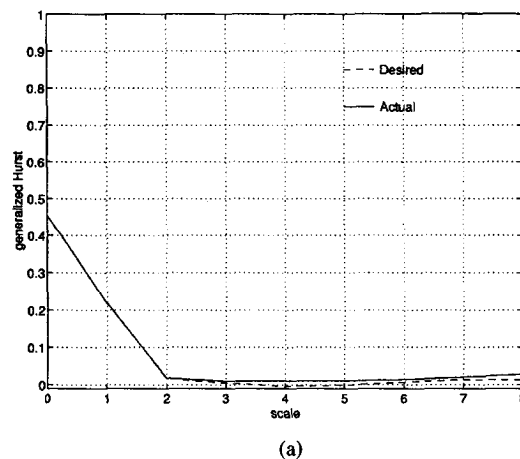

(a)

(b)

Fig. 10. Generalized Hurst parameters for pressed cork: (a) $\tilde{H}(m)$ and (b) $\tilde{H}_\Delta(s)$.
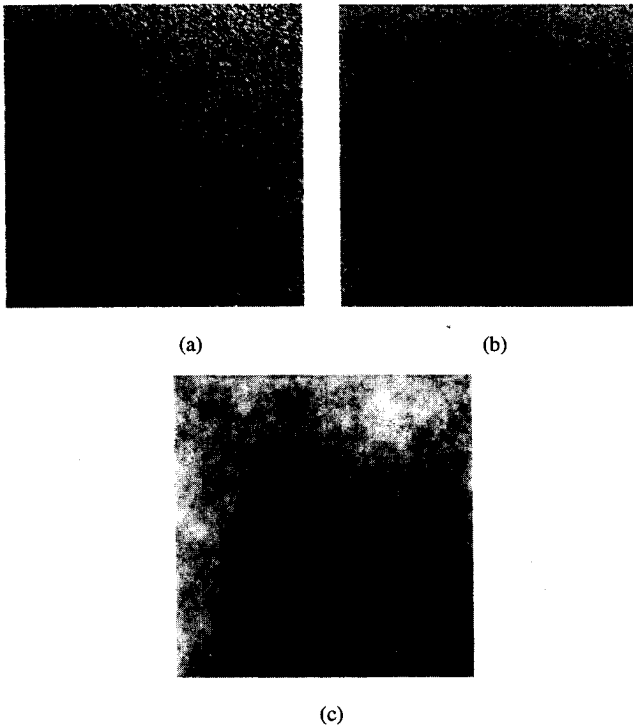
(a)   (b)

(c)

Fig. 11. Comparison of real and synthesized pressed cork textures: (a) pressed cork, (b) synthesized ESS model, and (c) synthesized fBm model ($H = 0.13$).

VIII. CONCLUSIONS AND EXTENSIONS

The concept of fBm has been generalized to allow for a wider range of natural textures and landscapes to be synthesized. It has been demonstrated how some different coastline features can be generated by different ESS models. For instance, the new approach allows an artist to choose the parameters of the afBm or the delta Hurst model to control how rugged the bays and peninsulas appear at different scales. Moreover, the artist can control the length and orientation of peninsulas by choosing a proper **R** matrix. We have demonstrated computationally simple algorithms to analyze and synthesize a class of natural textures using the ESS model. The ESS model and associated algorithms should prove equally useful for texture classification.

The theory of extended self-similar processes has many open problems. A study on necessary conditions for the generalized Hurst parameters would be very helpful. For example, results in [13] suggest that the differential Hurst parameter of (2.4) should be continuous. Furthermore, a detailed psychophysical study would help to further understand the strengths and weaknesses of the generalized Hurst values as a multiscale roughness measure. More application oriented studies include the use of the generalized Hurst parameter measurements for texture classification. To facilitate texture analysis applications, it would be of great interest to investigate the performance of the generalized Hurst parameter estimation algorithm on nonisotropic data and to extend the rendering method to nonisotropic textures. While the estimation of $\tilde{H}(m)$ for various orientations is straightforward, finding

a structure function model and **R** matrix to fit the $\tilde{H}(m)$ measurements along different orientations is a matter of further investigation. Finally, a study of methods to interpolate a 2D ESS process has important application to terrain modeling. The interpolation method may lead to faster synthesis algorithms and would allow for changes of the parameters of the ESS surface at different locations.

APPENDIX
PROOF OF THEOREM 2

PROOF OF (a). The fact that $\tilde{H}(m) \leq 1$ follows from Theorem 1.
The fact that $\tilde{H}_\Delta(s) < 1$ will be proved by induction. First $\tilde{H}_\Delta(1) \leq 1$ because $\tilde{H}_\Delta(1) = \tilde{H}(0)$. Now, assume that $\tilde{H}_\Delta(s) \leq 1$ for $s = 1, ..., n-1$ but $\tilde{H}_\Delta(n) > 1$. Then, we have

$$\frac{f(n+1)}{f(n)} > \frac{(n+1)^2}{n^2} \quad \text{and} \quad \frac{f(n)}{f(n-1)} \leq \frac{n^2}{(n-1)^2}.$$

Combining the two inequalities yields

$$\frac{f(n+1)+f(n-1)}{f(n)} > \frac{2n^2+2}{n^2}.$$

Then subtracting two from both sides and multiplying by $f(n)/2$ gives

$$\frac{r_X(n;1)}{\sigma^2} > \frac{f(n)}{n^2},$$

where $r_X(n; 1)$ is derived by (3.8). Since by (3.10) $f(n)$ can be expressed as a linear combination of $r_X(k; 1)$ that sums up to n^2 when $r_X(k; 1) = \sigma^2 \; \forall k$, one can show

$$r_X(n;1) > \sum_{k=0}^{n-1} a_k r_X(k;1),$$

where

$$\sum_{k=0}^{n-1} a_k = 1, \quad a_k \geq 0, \quad \forall k.$$

Therefore, one can conclude

$$r_X(n;1) > \min\{r_X(k;1): 0 \leq k \leq n-1\}.$$

However the inequality contradicts the hypothesis that $r_X(n;1)$ is monotonically decreasing. Thus, $\tilde{H}_\Delta(n) < 1$, and then by induction, $\tilde{H}_\Delta(s) \leq 1 \; \forall s$. A proof by induction is also used to provide the lower bounds for the generalized Hurst parameters. First, assume that $\tilde{H}_\Delta(1) < 1/2$. Then, we have $f(2) < 2f(1)$ which yields by (3.8) that $r_X(1; 1) < 0$. This contradicts the hypothesis. Next, assume that $\tilde{H}_\Delta(s) \geq 1/2$ for $s = 1, ..., n-1$, but $\tilde{H}_\Delta(n) < 1/2$. Then, we can write the following inequalities

$$\frac{f(n+1)}{f(n)} < \frac{n+1}{n} \quad \text{and} \quad \frac{f(n)}{f(n-1)} \geq \frac{n}{n-1},$$

which leads to

$$\frac{f(n+1) + f(n-1)}{f(n)} < 2.$$

Then by inspecting (3.8), it is easy to see that the inequality leads to the fact that $r_X(n; 1) < 0$. However, the incremental correlation is positive by hypothesis. Therefore $\tilde{H}_\Delta(n) > 1/2$, and then by induction $\tilde{H}_\Delta(s) \geq 1/2 \ \forall s$. To prove that $\tilde{H}_\Delta(m) > 1/2 \ \forall m$, we can write

$$\left(\frac{f(2^m+1)}{f(2^m)}\right)\left(\frac{f(2^m+2)}{f(2^m+1)}\right)\cdots\left(\frac{f(2^{m+1})}{f(2^{m+1}-1)}\right)$$
$$\geq \left(\frac{2^m+1}{2^m}\right)\left(\frac{2^m+2}{2^m+1}\right)\cdots\left(\frac{2^{m+1}}{2^{m+1}-1}\right).$$

Thus, $f(2^{m+1})/f(2^m) \geq 2$, and $\tilde{H}_\Delta(m) \geq 1/2 \ \forall m$.

PROOF OF (b). The fact that $\tilde{H}(m)$, $\tilde{H}_\Delta(s) \leq 1/2$ can be proved by using a similar technique as given in Part (a) and is therefore left to the reader. To prove the lower bound, we notice that since $r_X(k; 1)$ must have a positive spectrum and $r_X(k; 1) \leq 0$ for $k > 0$, then

$$r_X(0; 1) + 2\sum_{k=1}^{n+1} r_X(k; 1) \geq 0 \quad \forall n \in \mathbf{N}.$$

By using (3.9) it is easy to see that $f(n+1)/f(n) \geq 1$ and $\tilde{H}_\Delta(n) \geq 0$. Finally, we can write

$$\left(\frac{f(2^m+1)}{f(2^m)}\right)\left(\frac{f(2^m+2)}{f(2^m+1)}\right)\cdots\left(\frac{f(2^{m-1})}{f(2^{m+1}-1)}\right) \geq 1.$$

Thus, $\tilde{H}(m) \geq 0$. □

## ACKNOWLEDGMENT

REFERENCES

[1] P. Brodatz, *Textures: A Photographic Album for Artist & Designers*. New York: Dover, 1966.

[2] C.J. Burdett and M. Desai, "Localized fractal dimension measurement in digital mammographic images," *Proc. SPIE*, vol. 2,094, pp. 141-151, 1993.

[3] B.B. Chaudhuri, N. Sarkar, and P. Kundu, "Improved fractal geometry-based texture segmentation technique," *IEE Proc.-E*, vol. 140, pp. 233-241, Sept. 1993.

[4] R. Chellappa and R.L. Kashyap, "Texture synthesis using 2D noncausal autoregressive models," *IEEE Trans. Acoustics, Speech, and Signal Processing*, vol. 33, no. 1, pp. 194-203, 1985.

[5] C.-C. Chen, J.S. Dapone, and M.D. Fox, "Fractal feature analysis and classification in medical imaging," *IEEE Trans. Medical Imaging*, vol. 8, pp. 133-142, June 1989.

[6] A. Davis, A. Marshak, W. Wiscombe, and R. Cahalan, "Multifractal characterizations of nonstationary and itermittency in geophysical fields: Observed, retrieved, or simulated," *J. Geophysical Research*, vol. 99, pp. 8,055-8,072, Apr. 1994.

[7] M. Deriche and A.H. Tewfik, "Signal modeling with filtered discrete fractional noise processes," *IEEE Trans. Signal Processing*, vol. 41, pp. 2,839-2,849, Sept. 1993.

[8] K.J. Falconer, *The Geometry of Fractal Sets*. New York: Cambridge Univ. Press, 1985.

[9] K.J. Falconer, *Fractal Geometry: Mathematical Foundations and Applications*. England: John Wiley and Sons, 1990.

[10] P. Flandrin, "On the spectrum of fractional Brownian motions," *IEEE Trans. Information Theory*, vol. 35, pp. 197-199, Jan. 1989.

[11] S. Höfer, H. Hannachi, M. Pandit, and R. Kumaresan, "Isotropic two-dimensional fractional Brownian motion and its application in ultrasonic analysis," *Proc. 14th IEEE Eng. in Medicine and Biology Soc. Conf.*, pp. 1,267-1,269, 1992.

[12] J.R.M. Hosking, "Fractional differencing," *Biometrika*, vol. 68, no. 1, pp. 165-176, 1981.

[13] L.M. Kaplan, "Fractal signal modeling: Theory, algorithms, and applications," PhD dissertation, Univ. of Southern California, 1994.

[14] L.M. Kaplan and C.-C.J. Kuo, "Extending self-similarity for fractional Brownian motion," *IEEE Trans. Signal Processing*, vol. 42, pp. 3,526-3,530, Dec. 1994.

[15] L.M. Kaplan and C.-C.J. Kuo, "An improved method for two-dimensional self-similar image synthesis," Technical Report SIPI 249, Univ. of Southern California, June 1994. (to appear in *IEEE Trans. Image Processing*).

[16] L.M. Kaplan and C.-C.J. Kuo, "Fast image synthesis using an extended self-similar (ESS) model," *IEEE ICASSP-95*, vol. 4, pp. 2,575-2,578, May 1995.

[17] R.L. Kashyap and K.-B. Eom, "Texture boundary detection based on the long correlation model," *IEEE Trans. Pattern Analysis and Machine Intelligence*, vol. 11, pp. 58-67, Jan. 1989.

[18] R.L. Kashyap and P.M. Lapsa, "Synthesis and estimation of random fields using long-correlation models," *IEEE Trans. Pattern Analysis and Machine Intelligence*, vol. 6, pp. 800-809, Nov. 1984.

[19] J.M. Keller, S. Chen, and R.M. Crownover, "Texture description and segmentation through fractal geometry," *Computer Vision, Graphics, and Image Processing*, vol. 45, pp. 150-166, 1989.

[20] M.S. Keshner, "$1/f$ noise," *Proc. IEEE*, vol. 70, pp. 212-218, Mar. 1982.

[21] B. Klinkenberg and M.F. Goodchild, "The fractal properties of topography: A comparison of methods," *Earch Surface Processes and Landforms*, vol. 17, pp. 217-234, May 1992.

[22] T. Kumar, P. Zhou, and D.A. Glaser, "Comparison of human performance with algorithms for estimating fractal dimension of fractional Brownian statistics," *J. Optical Soc. of Am. A*, vol. 10, pp. 1,136-1,146, June 1993.

[23] J.P. Lewis, "Generalized stochastic subdivision," *ACM Trans. Graphics*, vol. 6, pp. 167-190, July 1987.

[24] T. Lundahl, W.J. Ohley, S.M. Kay, and R. Siffert, "Fractional Brownian motions: A maximum likelihood estimator and its application to image texture," *IEEE Trans. Medical Imaging*, vol. 5, pp. 152-161, Sept. 1986.

[25] S. Mallat and W.L. Hwang, "Singularity detection and processing with wavelets," *IEEE Trans. Information Theory*, vol. 38, pp. 617-643, Mar. 1992.

[26] Mandelbrot, *The Fractal Geometry of Nature*. San Francisco, Freeman, 1982.

[27] Mandelbrot and J.W. Van Ness, "Fractional Brownian motions, fractional noises, and applications," *SIAM Review*, vol. 10, pp. 422-437, Oct. 1968.

[28] Peitgen and D. Saupe, eds., *The Science of Fractal Images*. New York: Springer-Verlag, 1988.

[29] S. Peleg, J. Naor, R. Hartley, and D. Avnir, "Multiple resolution texture analysis and classification," *IEEE Trans. Pattern Analysis and Machine Intelligence*, vol. 6, pp. 518-523, July 1984.

[30] A.P. Pentland, "Fractal-based description of natural scenes," *IEEE Trans. Pattern Analysis and Machine Intelligence*, vol. 6, pp. 661-674, Nov. 1984.

[31] C.V. Stewart, B. Moghaddam, K.J. Hintz, and L.M. Novak, "Fractional Brownian motion models for synthetic aperture radar imagery scene segmentation," *Proc. IEEE*, vol. 81, pp. 1,511-1,522, Oct. 1993.

[32] A.M. Yaglom, *Correlation Theory of Stationary and Related Random Functions*. New York: Springer-Verlag, 1987.

[33] N. Yokoya, K. Yamamoto, and N. Funakubo, "Fractal-based analysis and interpolation of 3D natural surface shapes and their application to terrain modeling," *Computer Vision, Graphics, and Image Processing*, vol. 46, pp. 284-302, 1989.
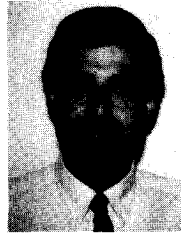
Lance M. Kaplan received the BS degree with distinction from Duke University, Durham, North Carolina, in 1989, and the MS and PhD degrees from the University of Southern California, Los Angeles, in 1991 and 1994, respectively, all in electrical engineering.

Dr. Kaplan held a National Science Foundation graduate fellowship and a USC Dean's Merit fellowship from 1990-1993, and worked as a research assistant in the Signal and Image Processing Institute at the University of Southern California from 1993-1994. He joined the Reconnaissance Systems Department of Hughes Aircraft Company in 1994. His research interests include fractal analysis, modeling and synthesis, image processing, multiresolution analysis, synthetic aperture radar, and remote sensing.

Dr. Kaplan is a member of Tau Beta Pi and Eta Kappa Nu.

C.-C. Jay Kuo received the BS degree from National Taiwan Unversity, Taipei, in 1980, and the MS and PhD degrees from the Massachusetts Institute of Technology, Cambridge, in 1985 and 1987, respectively, all in electrical engineering.

From October 1987 to December 1988 he was Computational and Applied Mathematics (CAM) research assistant professor in the Department of Mathematics at the University of California, Los Angeles. Since January 1989 he has been with the Department of Electrical Engineering-Systems and the Signal and Image Processing Institute at the University of Southern California, where he has a joint appointment as associate professor of electrical engineering and mathematics. His research interests are in the areas of digital signal and image processing, video coding, wavelet theory and applications, multimedia technologies, and alrge-scale scientific computing. He has contributed more than 170 technical publications to journals and conferences.

Dr. Kuo is a member of Sigma Xi, SIAM, SPIE, and the ACM, and a senior member of IEEE. He serves as associate editro for *IEEE Transactions on Image Processing* and *IEEE Transactions on Circuits and Systems: Video Technology* and is a member of the editorial borad of the *Journal of Visual Communication and Image Representation*. Dr. Kuo received the National Science Foundation Young Investigator award (NYI) and Presidential Faculty Fellow (PFF) award in 1992 and 1993, respectively.